Characterization of an Enzymatic Packed-Bed Microreactor: Experiments and Modeling

Filip Strniša, Marijan Bajić, Peter Panjan, Igor Plazl, Adama Marie Sesay, Polona Žnidaršič-Plazl

PII: S1385-8947(18)30817-9
DOI: https://doi.org/10.1016/j.cej.2018.05.028
Reference: CEJ 19044

To appear in: *Chemical Engineering Journal*

Received Date: 17 February 2018
Revised Date: 4 May 2018
Accepted Date: 5 May 2018

Please cite this article as: F. Strniša, M. Bajić, P. Panjan, I. Plazl, A.M. Sesay, P. Žnidaršič-Plazl, Characterization of an Enzymatic Packed-Bed Microreactor: Experiments and Modeling, *Chemical Engineering Journal* (2018), doi: https://doi.org/10.1016/j.cej.2018.05.028

Characterization of an Enzymatic Packed-Bed Microreactor: Experiments and Modeling

Filip Strniša [a,†], Marijan Bajić [a,†], Peter Panjan [b], Igor Plazl [a], Adama Marie Sesay [b], Polona Žnidaršič-Plazl [a,*]

[a] *Faculty of Chemistry and Chemical Technology, University of Ljubljana, Večna pot 113, 1000 Ljubljana, Slovenia*

[b] *Measurement Technology Unit, University of Oulu, Kehräämöntie 7, 87400 Kajaani, Finland*

Abstract

A micro packed-bed reactor (μPBR) based on two-parallel-plates configuration with immobilized *Candida antarctica* lipase B in the form of porous particles (Novozym® 435) was theoretically and experimentally characterized. A residence time distribution (RTD) within μPBRs comprising various random distributions of particles placed in one layer was computationally predicted by a mesoscopic lattice Boltzmann (LB) method. Numerical simulations were compared with measurements of RTD, obtained by stimulus-response experiment with a pulse input using glucose as a tracer, monitored by an electrochemical glucose oxidase microbiosensor integrated with the reactor. The model was validated by a good agreement between the experimental data and predictions of LB model at different conditions.

† Both authors equally contributed to the manuscript.

* Corresponding author. Tel: +386 1 479 8572

E-mail address: polona.znidarsic@fkkt.uni-lj.si

The developed μPBR was scaled-up in length and width comprising either a single or two layers of Novozym® 435 particles and compared regarding the selected enzyme-catalyzed transesterification. A linear increase in the productivity with the increase in all dimensions of the μPBR between two-plates demonstrated very efficient and simple approach for the capacity rise. Further characterization of μPBRs of various sizes using the piezoresistive pressure sensor revealed very low pressure drops as compared to their conventional counterparts and thereby great applicability for production systems based on numbering-up approach.

Keywords: packed-bed microreactor, biocatalysis, transesterification, residence time distribution, lattice Boltzmann, glucose biosensor

1. Introduction

Modern industrial practice irrepressibly strives towards the downsizing of the working equipment as a promising tool for the process intensification, and hence fast development, because miniaturized devices offer favorable mass and heat transfer rates due to a high surface-to-volume ratio stemming from their small dimensions [1]. Merging of continuously operated miniaturized reactors with biocatalytic processes has been growing steadily over the last decade, especially during bioprocess development stages [2,3 and refs. therein]. Immobilization of whole cells [4–6] or enzymes [7–9 and refs. therein] in microreactors could bring additional benefit due to easier isolation of products from the biocatalyst and the possibility for long-term biocatalyst use without the need for membrane-based separation.

Continuously operated miniaturized packed-bed reactors are proved to provide high biocatalyst loads and relatively long operational stability [5,8,10]. In order to efficiently increase reactor capacity and at the same time retain benefits of microscale processing, a one-dimensional scale-up of a μPBR with hydrogel particles containing amine transaminase was recently proposed [10]. It was also confirmed that the reactor performance strongly rely on fluid flow distribution within the packed bed [10]. However, hydrodynamic studies comprising flow regimes, pressure drop and RTD within μPBR are relatively rare, and tools for the characterisaton are typically sought among those used for the large scale packed-bed reactors [11]. Therefore the application of compatible, equi-scaled analytical devices is highly desirable to push this technology towards the “synergy of miniaturization” [12]. In this respect, biosensors are taking special place as powerful analytical tools that utilize a biological recognition component enabling rapid and selective on-line detection and quantification analytes. Diverse types of biosensors ranging from

optical to electrochemical ones are used for clinical, pharmaceutical and environmental analytes, as well as for monitoring of bioprocess parameters [13–15].

The LB method is a mesoscopic method used mainly for modeling of hydrodynamics, although its use extends well beyond that [16–18]. A major advantage that LB holds over the conventional computational fluid dynamics (CFD) methods such as finite volume, finite element and similar, is in the simplicity of incorporation of complex geometries [19]. This is especially suitable for the modeling of μPBR which, unlike the reactors with a single empty microchannel [20,21], have complex fluid flow patterns occurring in the interstices around the packed material. There have been attempts to use LB methods for simulation of the flow field with solute transport [19,22–24], and chemical reaction [22–24] within conventional packed-bed devices. However, an accurate LB-based simulation of solute transport remains a challenge, especially in systems where molecular diffusivity of the solute is very low [24].

The purpose of this work was computational and experimental evaluation of a μPBR containing porous resins with immobilized *Candida antarctica* lipase B (Novozym® 435). Previously developed packed-bed reactor concept between two plates [7,10] was utilized to assemble a μPBR with a single layer of Novozym® 435 particles. RTD in various randomly packed μPBR configurations was first modeled by mesoscopic LB method and further validated using a stimulus-response experiment with a pulse input and in-line monitoring comprising miniaturized biosensor. The μPBR was further scaled-up comprising either a single or two layers of Novozym® 435 particles and compared regarding the enzyme-catalyzed reaction. Transesterification of vinyl butyrate (VB) and 1-butanol (BUT) into butyl butyrate (BB) – an industrially important short-chain ester that resembles a pineapple aroma [7 and ref. therein] – and acetaldehyde (ACE) was used as a model reaction, for which the estimation of a temperature

optimum was also performed using selected µPBR. Furthermore, µPBRs of various geometries were characterized by means of pressure drop measurements using a piezoresistive pressure sensor.

2. Materials and Methods

2.1.Materials

Vinyl butyrate, 1-butanol, butyl butyrate, *n*-heptane, D-(+)-glucose, phosphate buffered saline (PBS) tablets, iron (III) chloride, glutaraldehyde, glucose oxidase (GOx) from *Aspergillus niger* VII S (E.C. 1.1.3.4), bovine serum albumin (BSA), and Nafion® 117 were of analytical grade and sourced from Sigma Aldrich (Steinheim, Germany). Hydrochloric acid was purchased from Merck Millipore (Darmstadt, Germany) and potassium ferricyanide from J.T. Baker (Deventer, The Netherlands). Glucose biosensors were based on screen printed electrodes purchased from ECOBIO lab (Florence, Italy).

A non-compressible polytetrafluoroethylene (PTFE) stripe DASTAFLON® 1620 was purchased from Dastaflon (Medvode, Slovenia), while expanded PTFE film (ePTFE) was sourced from GORE-TEX® (Gore & Associates, Inc., Newark, USA). Perfluoroalkoxy (PFA) tubes (0.5 mm ID; 1.59 mm OD) and high-pressure polyetheretherketone (PEEK) tube fittings were purchased from Vici AG International (Schenkon, Switzerland). A polyester double-sided adhesive tape ARcare® 90445 was kindly donated by Adhesives Research, Inc. (Limerick, Ireland).

The commercially available preparation Novozym® 435 having 1-2% (w/w) of moisture and containing 10% (w/w) of immobilized *Candida antarctica* lipase B (CaLB) with a nominal catalytic activity of 10,000 PLU g^{-1} (PLU stands for Propyl Laurate Unit – the amount of

enzyme activity which generates 1 µmol of propyl laurate per minute under defined standard conditions) was kindly donated by Novozymes A/S (Bagsværd, Denmark).

Milli-Q® water was used throughout the experiments.

2.2. Micro packed-bed reactor assembly

The main principles of the channel fabrication and µPBR assembly were described previously [10]. Briefly, a double-sided adhesive tape was cut off and placed to cover the entire surface of a bottom poly(methyl methacrylate) (PMMA) plate. Channels of various dimensions were then carved out from a 0.5 mm thick ePTFE film by means of a scalpel and adhered to the upper side of the adhesive tape. This was followed by adding two sheets of 0.1 mm and 0.3 mm thick non-compressible PTFE stripes as outer spacers, providing desired fixed channel depth of 0.4 mm. Novozym® 435 particles were then manually loaded into the channel and gently pushed down by a stainless steel laboratory spatula to stick on the adhesive tape and to prevent their leaching from the reactor. The excess of particles was carefully removed using a little soft brush in order to provide a one-layer bed. The upper PMMA plate having inlet and outlet holes connected to PFA tubes via high-pressure PEEK tube fittings was carefully placed on the top and sealed using screws. The same principle was applied for the reactor with two layers of particles with the fact that the adhesive tape was placed on the upper PMMA plate as well. PMMA plates of 10 cm × 5 cm × 1.5 cm regarding length, width and depth, respectively, were used to assemble the rectangular reactors approximately 3 mm in width, hereinafter reffered to as basic channel, while plates of 15.7 cm × 6.6 cm × 1.5 cm were applied for the reactors with triangular inlet and outlet distributors or pre-chambers. An illustration of a general µPBR assembly is shown in Figure 1a.

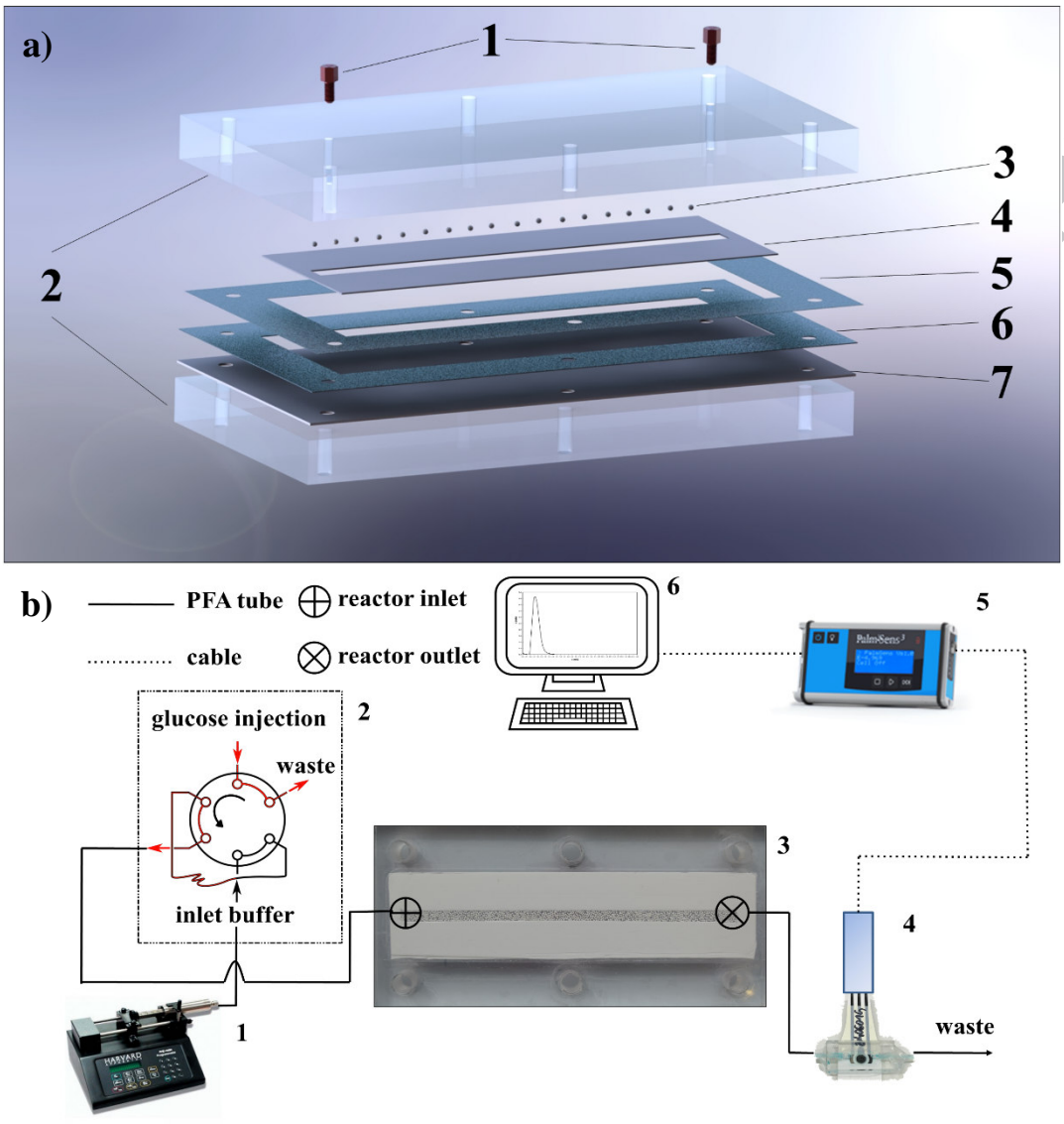

Figure 1. a) Assembling and the main parts of a µPBR with Novozym® 435: 1) high pressure tube fittings; 2) PMMA plates; 3) schematic display of a minor fraction of Novozym® 435 particles within the reaction channel; 4) ePTFE gasket; 5) 0.1 mm thick non-compressible PTFE spacer; 6) 0.3 mm thick non-compressible PTFE spacer; 7) thin polyester double-sided adhesive tape. b) Schematic of the test loop for the stimulus-response experiment with the pulse input: 1) syringe pump; 2) HPLC injection valve; 3) µPBR; 4) glucose biosensor; 5) PalmSens potentiostat; 6) computer for recording the output signal.

2.3. Residence time distribution measurements

RTD analysis within μPBRs with a single layer of particles was performed by a stimulus-response experiment with a pulse input [25], using glucose as a non-reactive tracer. In-line monitoring of glucose concentration at the μPBR outflow was done by an electrochemical glucose oxidase biosensor fabricated as reported previously [14]. The biosensor has been integrated into a CO_2-laser cut PMMA chip of 4 μL internal volume. Amperometric signals of the glucose oxidase biosensor have been read by a PalmSens3 potentiostat (PalmSens, Houten, The Netherlands).

The experimental test loop assembled for the stimulus-response experiment with the pulse input is shown in Figure 1b. PBS (100 mM; pH 7.4) was continuously supplied at 24 ºC in a temperature-controlled room through the system interconnected with PFA tubes using a Harvard Apparatus PHD 4400 high pressure pump (Harvard Apparatus, Holliston, USA) at the flow rate of 100 μL min^{-1}. 10 μL of 50 mM glucose solution (total load 5×10^{-4} mmol) in PBS was instantaneously injected in the system using an HPLC injection valve (Knauer, Berlin, Germany) [26], connected to the pump as shown in Figure 1b. Glucose concentration was measured at the reactor outlet at various times using a calibrated biosensor with the measurement frequency of 10 Hz. Due to the high quantity of data, an average for every 10 measurements was calculated, and the yielding values were used to generate the pulse-response curve. The experiments were performed in triplicates.

The mean residence time (τ), variance (σ^2) and skewness (s) of the distribution $C_{glu}(t)$ were calculated from the pulse-response measurements as stated in the literature [27]. The starting assumptions involved the closed vessel boundary conditions (the fluid enters and leaves the reactor only once and there is no recirculation), steady state flow, homogeneous system, an inert tracer which does not disturb the flow, and isothermal conditions [28].

2.4. Preparation and characterization of Novozym® 435

To obtain the particles with narrow size distribution, Novozym® 435 was consecutively sieved through the sieves with pore sizes of 500, 425 and 300 μm. Each fraction was then analyzed under the light microscope (Leica Microsystems, Wetzlar, Germany) equipped with a photo camera (Nikon D5100, Tokyo, Japan). The average particle diameter was determined based on the image analysis of cca. 300 spherical particles using the ImageJ software (National Institutes of Health, Bethesda, USA).

The activity of Novozym® 435 with immobilized CaLB was determined in batch runs using the initial rate method. Measurements were carried out at 24 ºC using test tubes continuously stirred on a magnetic stirrer IKA® RCT (IKA-Werke GmbH & Co. KG, Staufen, Germany) at 800 rpm. The reaction mixture (2 mL) was an equimolar 600 mM solution of VB and BUT in *n*-heptane. The concentration of Novozym® 435 in the vessel (C_{N435}) was set to 5 g_{N435} L^{-1} in order to reach the final CaLB concentration (C_{CaLB}) of 0.5 $g_{CaLB}L^{-1}$. The assays were performed in duplicates.

BB concentration in the withdrawn samples was followed over the time and the activity was calculated from its linear increase. Specific activity was expressed either per mass of Novozym® 435 [U mg_{N435}^{-1}], or per mass of enzyme [U mg_{CaLB}^{-1}], while U was defined based on the synthesis of 1 μmol of BB per min under described conditions.

2.5. Biotransformations in μPBRs

Transesterification reactions were performed by pumping an equimolar 600 mM solution of VB and BUT in *n*-heptane at flow rates ranging from 12.2 μL min^{-1} to 3,756.3 μL min^{-1} through the

μPBRs with and without triangular pre-chambers of different sizes as described in Results section. Reactors were randomly packed with various amounts of Novozym® 435 (from 7.1 mg to 148.4 mg), yielding final enzyme loads (γ_{CaLB}) from 5.06 U μL^{-1} to 5.53 U μL^{-1}. After reaching the steady-state, at least two consecutive samples were taken from the outflow of the μPBR, collected in a closed vial to prevent evaporation, and analyzed as described below. The experiments were performed at 24 ºC.

The temperature effect on the transesterification process was evaluated by embedding the μPBR with a 23.93 mm long, 3.12 mm wide and 0.40 mm deep rectangular channel, packed with 7.1 mg of Novozym® 435 in one layer into a thermostated bath with automatic temperature control (Julabo, Seelbach, Germany). The flow rate was 170.7 μL min^{-1}, while the temperature varied from 24 to 80 (± 0.5) ºC.

Void volume (V_v) and bed porosity (ε) of μPBRs were estimated from the volume of empty channels calculated from their dimensions, and the volume of particles in the reactor calculated from their mass weighed using an analytical weighing machine (Mettler-Toledo Ltd., Leicester, UK, measured uncertainty: ± 0.5 × 10^{-4} g) and density (considered to be 0.555 mg μL^{-1} [29]). The mean residence time was further calculated as the ratio of V_v and applied volumetric flow rate (Q) [10]. Conversion (X) was calculated from the inlet and outlet concentration of BUT, while volumetric productivity (Q_p) and production rate (PR) were calculated using the outlet concentration of BB, V_v and τ, analogously with the equations described in our previous work [10]. Biocatalyst productivity number (BPN) was calculated as the ratio of the outlet concentration of BB and concentration of CaLB expressed per volume of the reaction solution.

2.6. Chemical analysis

A gas chromatograph HP 6890 (Hewlett-Packard, Palo Alto, USA) equipped with an HP-INNOWAX (30 m length × 0.25 mm ID × 0.5 µm film thickness) column (Agilent Technologies, Santa Clara, USA) was used to determine the concentration of VB, BUT and BB in *n*-heptane according to the procedure described elsewhere [21]. Retention times for VB, BUT and BB in the used column were 1.2 min, 1.4 min and 1.7 min, respectively. Concentrations of analytes were calculated from the calibration curves prepared from standard solutions.

2.7. Pressure drop measurements

Pressure drop in µPBRs of various geometries was measured by HMI Series Amplified pressure sensor HMIB001UZ5H5 from First Sensor AG (Berlin, Germany) and 2700 Keithley Multimeter/Data acquisition system. Measuring range of pressure sensor was 0-100 kPa with the total accuracy of ± 1.5%. Measurements were performed at 24 ºC using water at flow rates from 30 µL min^{-1} to 1,800 µL min^{-1}. [30]The pressure sensor was connected into the flow path by applying a T-junction, PFA tubes and high-pressure PEEK tube fittings resulting in a minimal dead volume [30].

3. Model development

Residence time distribution simulation of µPBR was done using two different 3-dimensional LB models. A model with 19 lattice velocities (D3Q19) was used to solve the velocity field, while a model with 7 lattice velocities (D3Q7) was used to solve the solute transport in order to accelerate the simulation without a major loss of accuracy [22]. The LB equation with the

Bhatnagar–Gross–Krook (BGK) approximation, which is the central part of the method, reads as follows [17]:

$$f_a(\boldsymbol{x} + \boldsymbol{e}_a\Delta t, t + \Delta t) - f_a(\boldsymbol{x}, t) = -\omega\left(f_a(\boldsymbol{x}, t) - f_a^{eq}(\boldsymbol{x}, t)\right), \quad (1)$$

where f is the distribution function, $\boldsymbol{x}$ represents the space coordinates, t is the time and $\boldsymbol{e}$ is a basic lattice velocity, while ω is the relaxation parameter. The index a takes a value between 0 and 18 for the D3Q19 model and indicates the equation's local discretization. The left hand side is a mathematical representation of the streaming step, and the right hand side is the BGK collision operator with a special equilibrium distribution function (f^{eq}) [18]:

$$f_a^{eq}(\boldsymbol{x}, t) = W_a\rho(\boldsymbol{x}, t)\left[1 + \frac{\boldsymbol{e}_a\cdot\boldsymbol{u}(\boldsymbol{x}, t)}{c^2} + \frac{1}{2}\frac{\left(\boldsymbol{e}_a\cdot\boldsymbol{u}(\boldsymbol{x}, t)\right)^2}{c^4} - \frac{1}{2}\frac{\boldsymbol{u}(\boldsymbol{x}, t)^2}{c^2}\right], \quad (2)$$

where c and W are the speed of sound and the lattice weight factor, respectively. Both depend on the lattice model utilized. In the D3Q19 model $c = \frac{1}{\sqrt{3}}$, and W_a equals to: $\frac{1}{3}$ for $a = 0$, $\frac{1}{18}$ for $a =$ 1,... 6, and $\frac{1}{36}$ for $a = 7$, ... 18. Furthermore, ρ is the local density and $\boldsymbol{u}$ is the local velocity. ρ can be computed by summing all the f at a node: $\rho(\boldsymbol{x}, t) = \sum_{a=0}^{18} f_a(\boldsymbol{x}, t)$, and $\boldsymbol{u}$ can be computed by finding the local momentum and dividing it by the density: $\boldsymbol{u}(\boldsymbol{x}, t) = \frac{1}{\rho(\boldsymbol{x},t)}\sum_{a=1}^{18} f_a(\boldsymbol{x}, t)\cdot\boldsymbol{e}_a$. When considering passive solute transport in LB, the same equations are used, but the equation for the equilibrium distribution function can take on a simpler form [24]:

$$g_a(\boldsymbol{x} + \boldsymbol{e}_a\Delta t, t+\Delta t) - g_a(\boldsymbol{x}, t) = -\omega_s\left(g_a(\boldsymbol{x}, t) - g_a^{eq}(\boldsymbol{x}, t)\right), \quad (3)$$

$$g_a^{eq}(\boldsymbol{x}, t) = \rho_s(\boldsymbol{x}, t)\left[\widetilde{W}_a + W_a\frac{\boldsymbol{e}_a\cdot\boldsymbol{u}(\boldsymbol{x}, t)}{c^2}\right], \quad (4)$$

where ω_s is solute's relaxation parameter, solute's distribution functions are marked as g to avoid confusion with solvent's distribution functions, and ρ_s denotes the local solute concentration. The index a takes values between 0 and 6 for the D3Q7 model. In the D3Q7 model $c = \frac{1}{\sqrt{4}}$, and W_a equals to: $\frac{1}{4}$ for $a = 0$, and $\frac{1}{8}$ for $a = 1,\ldots 6$. ρ_s can be determined similarly to ρ: by summing up all the g at a node: $\rho_s(\boldsymbol{x}, t) = \sum_{a=0}^{6} g_a(\boldsymbol{x}, t)$ Although simpler, g^{eq} depends on two different W, where $\widetilde{W}$ represents the modified lattice weight factors. This modification allows for simulation of systems with Schmidt number (Sc) up to 1000. Such systems are otherwise hard to simulate with BGK LB, because solvent's kinematic viscosity ($\nu = c^2\left(1/\omega - 0.5\right)$) and solute's molecular diffusivity ($D = 1/3\left(1 - \widetilde{W}_0\right)\left(1/\omega_s - 0.5\right)$) [24], both depend on their respective relaxation parameters. Since kinematic viscosity and molecular diffusivity cannot equal 0 or have negative values, ω and ω_s cannot be greater than or equal to 2. According to the literature, most stable values for ω are above 0.8 [24], and it should also be noted that stability decreases as ω approaches 2 [17]. This introduces a difficulty when simulating diffusion in liquid systems. Eq. 4 is a solution which allows high Sc values without having to use ω_s too close to 2.

To utilize the LB method, a solver was developed. The code was written in CUDA C++ programming language, to be executed on a graphics processing unit (GPU). A lattice of 2048 × 256 × 32 nodes was designed. Pixeled spheres with diameter 32 nodes were randomly packed in the rectangular geometry yielding various particles distributions (see supplementary material, Figure S1). Solid boundaries – channel walls and spherical particles – were defined by the simple half-way bounceback boundary condition. For the inlet and outlet, on west and east side of the system, respectively, Zou and He velocity and pressure boundary conditions were used, as

derived by Hecht and Harting for the 19 lattice velocity model [31,32]. Velocity profile at the inlet was set to plug flow at flow rate of lattice equivalent of 100 μL min^{-1}.

Once the program found the equilibrium solution of the velocity field, it started simulating the injection of the tracer via constant mass flux boundaries [17] for a lattice equivalent of 6 seconds, and after that it changed the mass flux at the inlet to 0. The simulation had 4 runs, where a random packing of spherical particles was created each run. The program recorded the concentration at 50 nodes after the inlet and 15 nodes before the outlet, to minimize the effects of the boundary conditions on the results.

4. Results and discussion

4.1. Residence time distribution

The resealable system of μPBR between two-plates, where the geometry and the dimensions of the packed-bed microchannel are defined by a cutout of the ePTFE gasket, and the thickness of a non-compressible PTFE spacer, enabled easy and efficient packaging of catalyst particles as shown in Figure 1a. Simple loading of Novozym® 435 allowed repeatable preparation of a μPBR with a single layer of randomly distributed particles yielding experimental bed porosity (ε) around 0.57 ± 0.02 (reactor A in Table 1). To provide a homogeneous packed bed, a polydisperse Novozym® 435 preparation was preliminarily sieved as stated in Section 2.4, and only the fraction with the diameter d_{N435} of 372.10 ± 27.05 μm was used throughout the study.

The residence time distribution of such μPBR was numerically simulated using the LB model described above. Computations ran on a desktop personal computer with Intel® Core™ i7-930 processor with 6 GB DDR3 RAM, and NVIDIA® GeForce® GTX 1060 6 GB GDDR5 GPU. The

code was compiled with NVIDIA® CUDA® Compiler from NVIDIA® CUDA® Toolkit 8.0 with G++ from GNU Compiler Collection 5.4 on Ubuntu 16.04 operating system. A random packing generator based on two input variables was written in the C++ programming language. It was used to manipulate the bed porosity. The first variable was controlling the minimal distance allowed between particles, and the other represented the probability of a particle center being positioned at a certain point. In all our generated beds, touching between particles was allowed, meaning that the minimal distance between them was set to 0. The probability variable was empirically tuned to obtain the desired bed porosity, and afterwards remained unchanged for all generated beds, which allowed the control of bed porosity values to the specific operational window. At constant input variables, the bed porosity would slightly vary from simulation to simulation. In four simulation runs performed, ε ranged between 0.570 and 0.578 (see Supplementary material, Figure S1). Simulation snapshots are presented in Figure 2. After completing RTD analysis for the selected physical domain of μPBR, an average τ obtained was 0.177 min and s was 0.57.

To validate the computational observations and further to characterize the setup of μPBR, the pulse tests were experimentally performed. A μPBR with the dimensions of the mesoscopic lattice model physical domain (reactor A in Table 1) was integrated with the electrochemical biosensor for in-line tracer analysis as shown in Figure 1b. Glucose oxidase-based biosensors developed to monitor glucose as a tracer in RTD analysis have been fully characterized before use. The measurement range was found to be linear up to 5 mM concentration, the detection limit was 0.006 mM and response times were sufficiently rapid for the nature of the experiments. Additionally, the stability of the biosensor has been assessed via thermally accelerated aging and was found to be sufficient for one-day measurements [14].

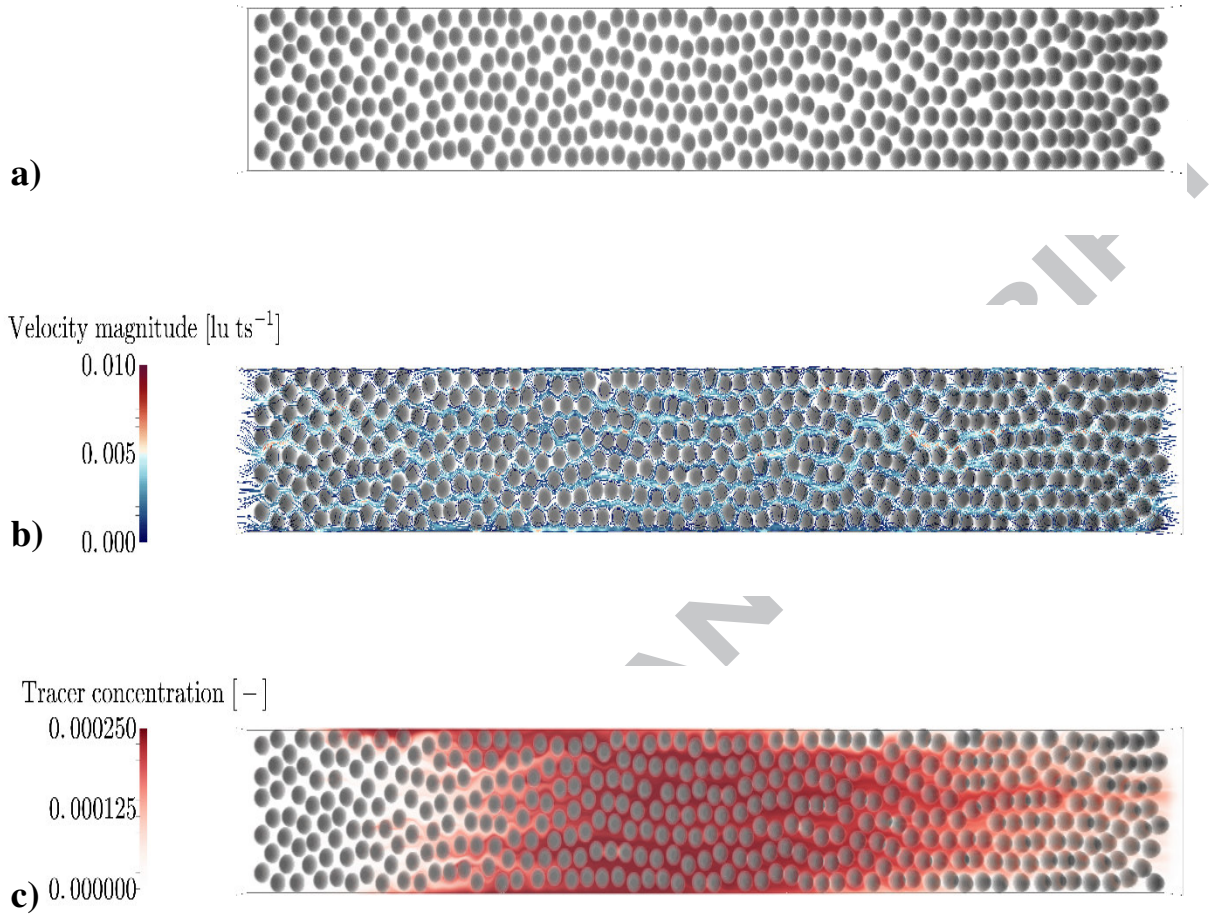

Figure 2. a) An example of computer-generated μPBR porous structure (ε = 0.570). b) A streamline representation of the velocity field in the porous structure as it was computed with LB. c) A volume representation of the tracer passing through the porous structure as it was computed with LB.

The computational and the experimental response curves of the tracer in the reactor A (Table 1) are presented in Figure 3a, where the displayed values are dimensionless glucose concentration (C/C_{max}) at the reactor outlet vs. dimensionless time (t/τ). A good agreement between measured and simulated response curve is observed for the case when the experimental porosity matched the numerically generated porosity of 0.57. This agreement, obtained without any fitting

procedure of LB model parameters, demonstrate the validation of mesoscopic computational description of hydrodynamic characteristics and transport phenomena in μPBR. Comparing the computational results in Figure 3a among themselves, it can be deduced, that the random packing of particles, as it is represented by slightly deviating values of ε, does not further affect the dispersion of the tracer. This is shown by the overlap of the response curves. The computer program that performed the simulations also recorded the concentration near the inlet (data not shown). These results were used in a control mass balance. The error recorded in mass balances was about 1 %. This is probably a consequence of using the modified BGK model described above at the edge of its numerical stability, which resulted in some local mass accumulation, which lead to global mass balance errors. Mass accumulation was especially noticeable at solid boundaries, where local concentration would exceed the inlet concentration (data not shown). This error may be minimized with a multi-relaxation collision scheme, and improved boundary conditions for solid walls. The location of the wall depends on ω, when bounceback boundaries are used in combination with BGK collision model. Ideally it is located half-way between a fluid and a solid node when $\omega = 1$ [33]. However, a test in an empty channel section has shown that walls in our simulations were located at 0.548 node towards the fluid (data not shown), buthe influence on the overall volume and porosity of the simulated channel was negliglible due to the estimated error below 1.5 %.

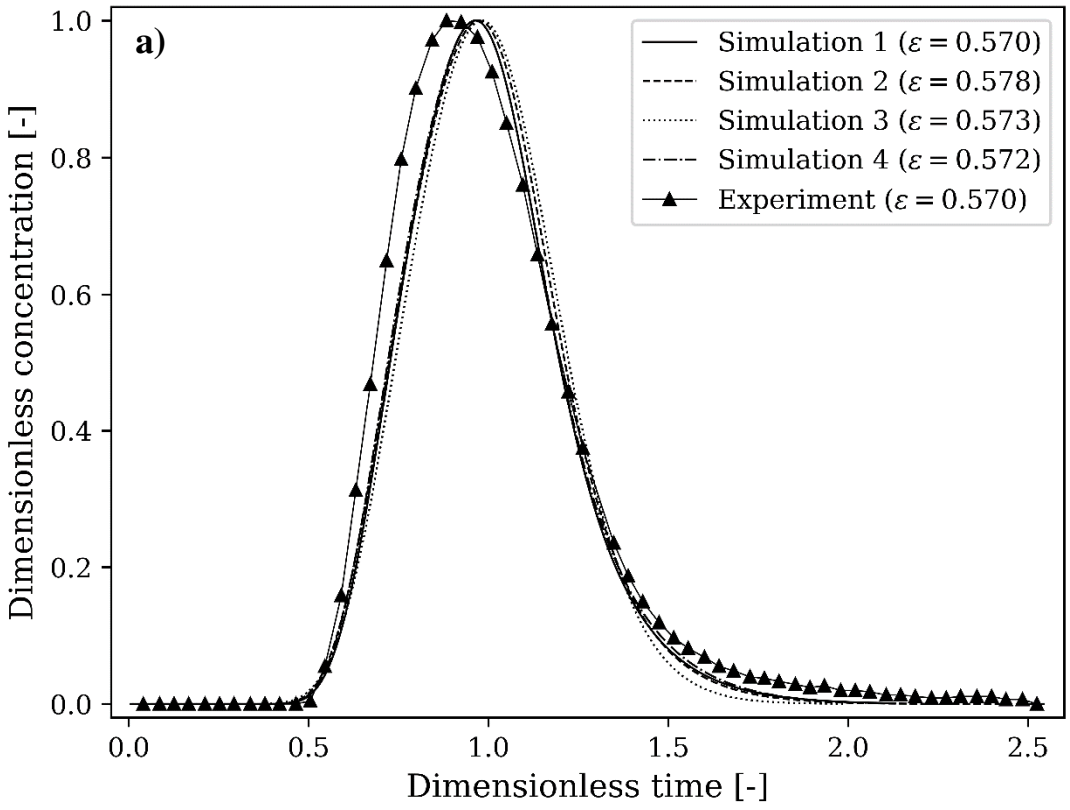

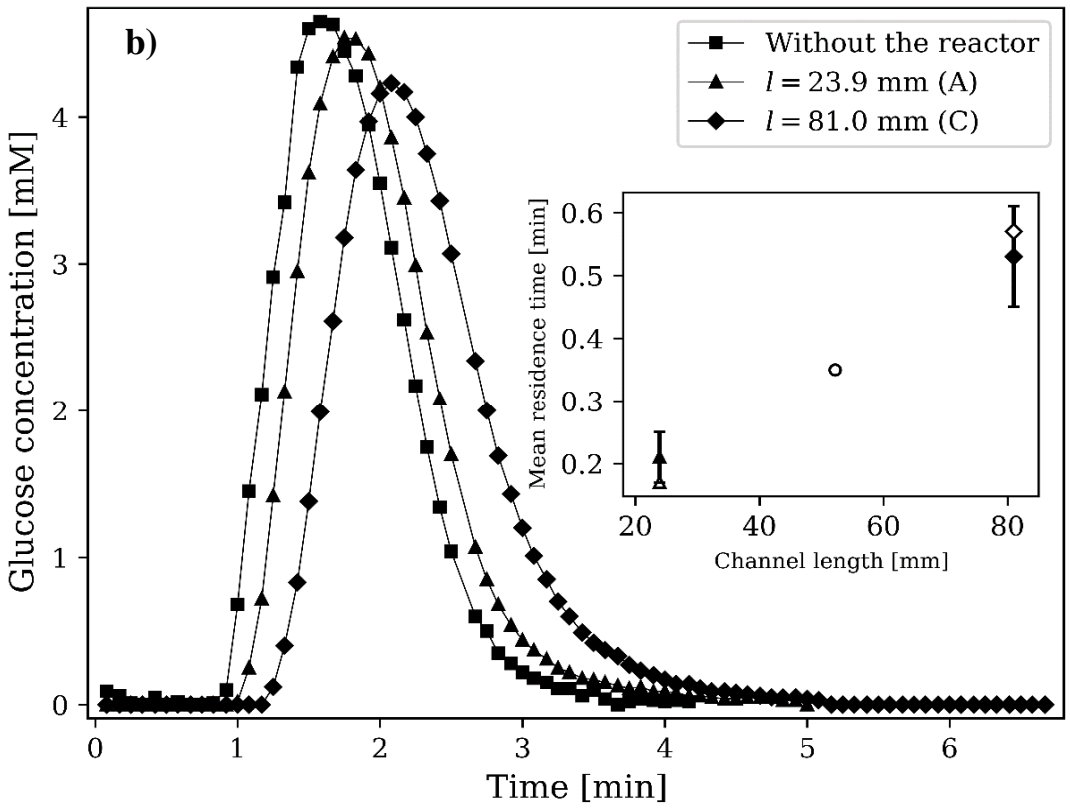

Figure 3. a) A comparison of experimental results and the LB model simulations of the reactor A described in Table 1 at different random packing of particles (see Figure S1). b) Pulse-response curves obtained in RTD analysis of μPBRs described in Table 1 together with estimated mean residence times. Empty and filled markers in the inset graph denote calculated and experimentally obtained mean residence times for the same μPBRs, respectively (○ is reactor B from Table 1). The experiments were performed by pumping 50 mM solution of glucose in 100 mM PBS (pH 7.4) at Q = 100 μL min^{-1} and T = 24 ºC.

RTD was further experimentally analyzed for an approximately 4-times longer channel of the same depth and similar width, filled with Novozym® 435 particles (reactor C in Table 1). Figure 3b presents the comparison of pulse-response curves and mean residence times for μPBRs of different lengths, calculated from theoretical predictions and experimental data. Besides, the pulse response without the reactor, where the glucose inlet was directly linked with the biosensor, was monitored. Very favorable hydrodynamics without any noticeable channeling is evident from Figure 3b. The detailed results of RTD analysis including particle Reynolds number (Re_p) indicating laminar flow for the reactors presented in Figure 3b are summarized in Table 1.

Table 1. Detailed results of RTD analysis: mean residence time (τ), variance (σ^2), skewness (s), axial dispersion coefficient ($\mathcal{D}$), and dispersion number ($\mathcal{D}/vl$) calculated from the pulse-response measurements. Also included in this table are channel dimensions: length (l), width (w) and height (h).

μPBR	***l***	***w***	***d***	***ε***	***Re_p***[a)]	***τ***	***σ^2***	***s***	***$\mathcal{D}\times 10^5$***	***$\mathcal{D}/vl$***
mark	**[mm]**	**[mm]**	**[mm]**	**[-]**	**[-]**	**[min]**	**[min^2]**	**[-]**	**[$m^2\ s^{-1}$]**	**[-]**
A	23.9	3.1	0.40	0.57	0.95	0.21	0.08	0.77	1.42	0.45

C	81.0	2.9	0.40	0.59	0.98	0.53	0.14	0.42	0.92	0.08

[a)]Calculated for Q = 100 µL min^{-1} based on the mean interstitial fluid velocity (v_i) estimated from the fluid velocity (v) and ε as well as d_{N435} and physical properties of water.

4.2.Enzyme-catalyzed transesterification in µPBRs of various geometries

The rectangular µPBR randomly packed with Novozym® 435 particles (Figure 4a) was further scaled-up in width. According to previous findings on the performance of the miniaturized packed-bed reactor with poly(vinyl alcohol) lens-shaped particles [10], a triangular shape with pillars at the inlet and outlet part was applied as shown in Figure 4b. Furthermore, a µPBR with an increased channel depth comprising 2 layers of particles, was prepared and µPBRs of various geometries were further tested regarding the selected transesterification. Characteristics and performance of tested µPBRs are summarized in Table 2.

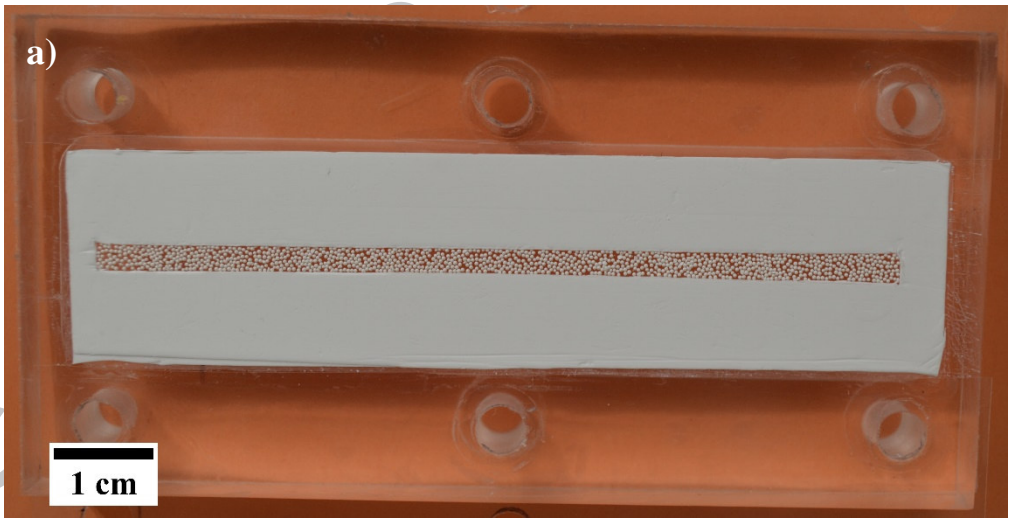

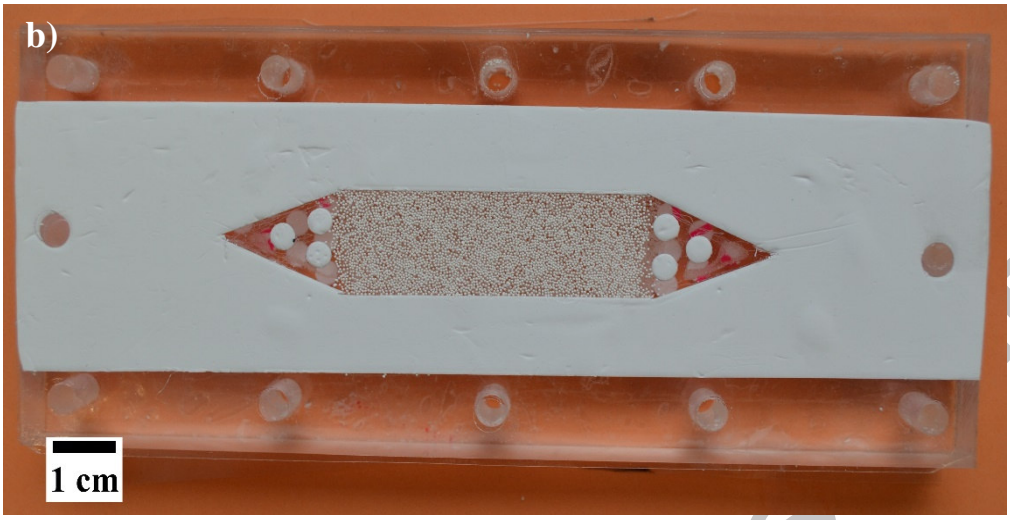

Figure 4. µPBRs randomly packed with one layer of Novozym® 435 in: a) basic channel (reactor C in Table 2); b) channel with triangular inlet and outlet parts containing pillars, referred to in text as "pre-chamber" (reactor D in Table 2).

Table 2. Characteristics and performance of tested µPBRs with Novozym® 435 at 24 °C.

µPBR *mark*	*l* [mm]	*w* [mm]	*d* [mm]	*No. of layers*[b)]	*V* [µL]	V_v[c)] [µL]	*ε* [–]	γ_{CaLB} [U µL^{-1}]	*BPN*[d)] [mmol$_{BB}$ g$_{CaLB}^{-1}$]
A	23.9	3.1	0.4	1	29.9	17.1	0.57	5.53	13.56
B	52.2	3.0	0.4	1	61.6	35.3	0.57	5.51	12.72
C	81.0	2.9	0.4	1	95.3	56.5	0.59	5.06	13.35
D	50.9	15.8[a)]	0.4	1	321.6	184.0	0.57	5.52	12.18
E	53.8	29.2[a)]	0.4	1	628.7	363.6	0.58	5.38	12.64

F	50.9	15.8[a)]	0.8	2	643.1	375.6	0.58	5.26	14.03

a) The values refer to the width of the rectangular part of the channel with triangular pre-chambers.

b) Number of Novozym® 435 layers placed one on top of the other within the channel depth.

c) Estimated from the reactor volume and volume of particles calculated from their mass and density.

d) Maximal *BPN* calculated at the longest mean residence time (τ = 1.4 min).

Bed porosities of tested µPBRs were between 0.57 and 0.59 (Table 2). This is close to the porosity of 0.64 reported for the µPBR with a 90 mm long, 5 mm wide and 0.448 mm deep rectangular channel packed with non-sieved Novozym® 435 particles having average diameter of 454 µm [7]. Enzyme load in assembled µPBRs was between 5.06 U $\mu L^{-1}$and 5.53 U μL^{-1}, which was calculated from the specific activity of Novozym® 435 used in µPBRs. This was preliminary evaluated in a batch experiment and was found to be 13.31 ± 0.27 U mg_{N435}^{-1}, which based on the estimation of 10 % (w/w) of CaLB in the preparation [7] corresponds to 133.05 ± 2.71 U mg_{CaLB}^{-1}.

An equimolar 600 mM solution of VB and BUT in *n*-heptane was pumped through the µPBRs at various flow rates described below. Results of transesterification reaction expressed as conversions calculated from the substrate concentration at the inlet and outlet of the µPBRs, as well as production rates calculated at the longest mean residence times are summarized in Figures 4a-c.

The µPBRs of various lengths consisted of one layer of Novozym® 435 and with approximately the same width were first tested at flow rates ranging from 12.2 µL min^{-1} to 565.2 µL min^{-1} to achieve the mean residence times from 0.1 min to 1.4 min. As evident from Figure 5a, there is a

linear relationship between the channel length and the production rate of the reactor (R^2 = 0.9991). As expected, all tested µPBRs performed equally at the same mean residence times and the maximal conversion of approximately 95% was obtained in less than 0.8 min (Figure 5a).

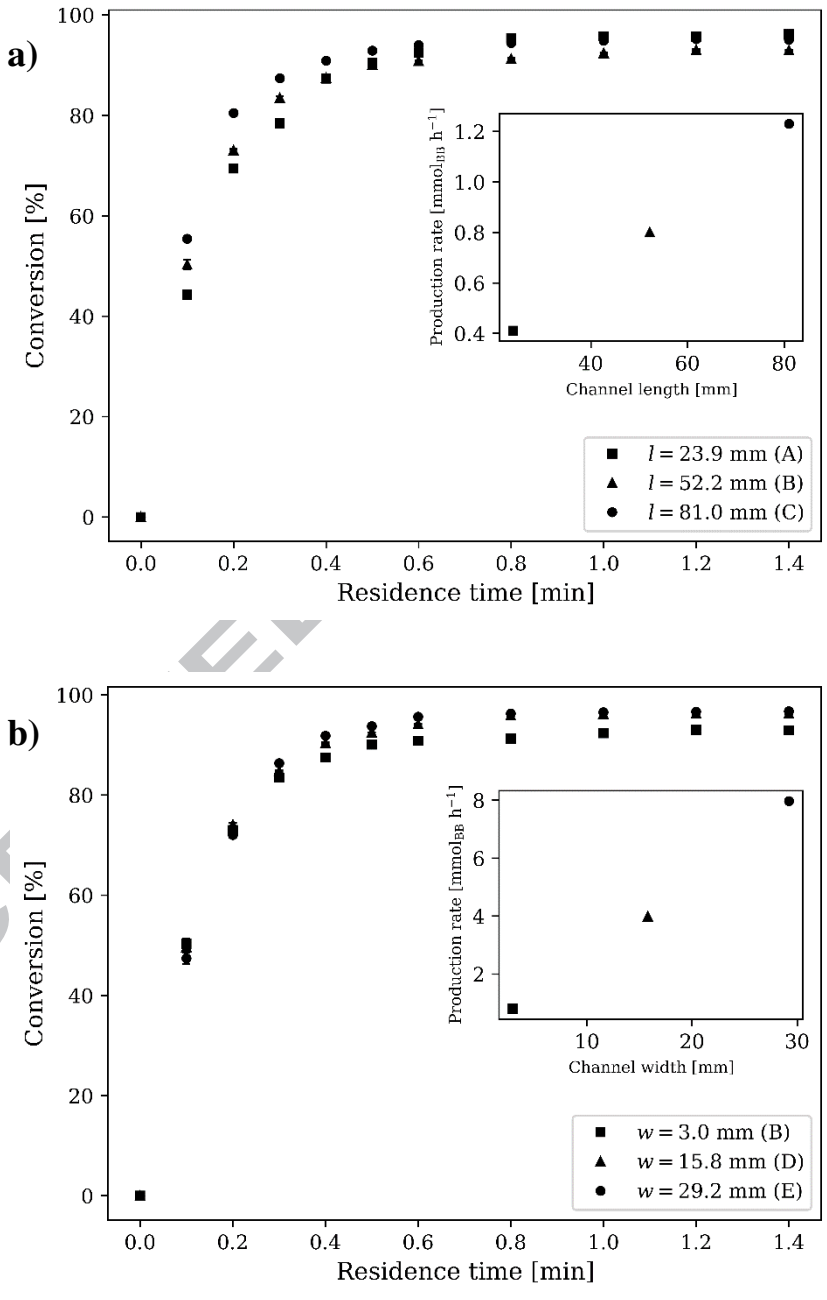

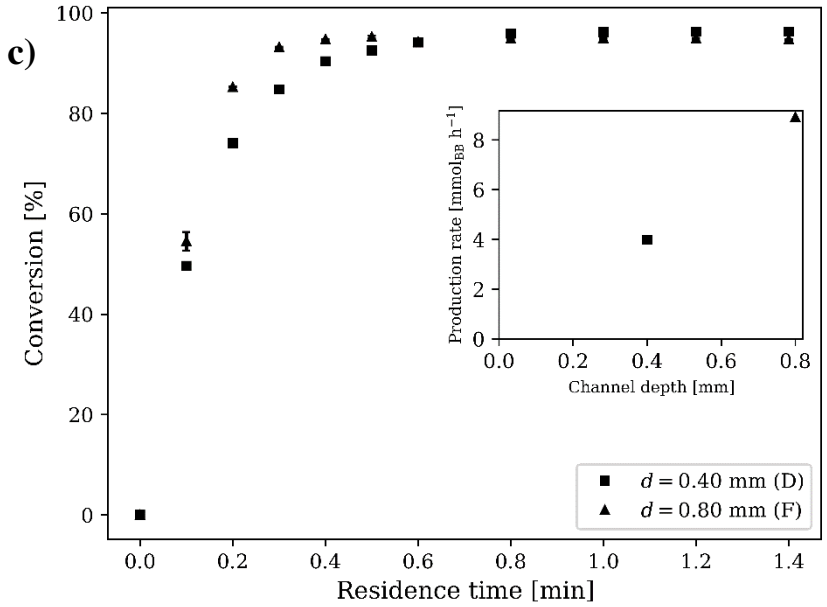

Figure 5. Impact of channel length (a), width (b) and depth (c) on substrate conversion at the µPBRs outlets at various flow rates and thereby mean residence times together with production rates estimated at the longest mean residence time (maximal conversion) in the µPBRs without (A, B, C) and with triangular pre-chambers (D, E, F) randomly packed in one layer with Novozym® 435. Other µPBRs characteristics are presented in Table 2. The reactions were performed by continuous pumping of 600 mM equimolar inlet concentration of VB and BUT in *n*-heptane, at 24 ºC.

To increase the productivity and at the same time maintain the ideal hydrodynamic properties and efficiency of the µPBR channel, the selected transesterification process was further conducted in the µPBRs with the wider channels containing triangular pre-chambers with pillars (Figure 5b). Such configuration was shown to efficiently distribute the inlet fluid flow and thus maintains the hydrodynamics of the basic channel [10]. The flow rates were set to range from 25.2 µL min^{-1} to 3,636.4 µL min^{-1} in all three µPBRs to achieve the mean residence times from 0.1 min to 1.4 min.

The maximal conversion was again achieved within less than 0.8 min in all tested μPBRs, while the production rate estimated at the most extended mean residence time kept its linearity (R^2 = 0.9974) with increasing channel width (Figure 5b). The μPBR with the widest channel achieved approximately 10-times higher production rate than the μPBR with the narrowest channel (inset graph in Figure 5b). The achieved BPNs were revolving around 12.51 $mmol_{BB}\ g_{CaLB}^{-1}$ for all three μPBRs with the consecutively wider channels (reactors D, E and F in Table 2).

The effect of the channel depth on the reactor performance was examined using two μPBRs with triangular pre-chambers of the same length and width, and with the pre-chambers containing pillars. Both were randomly packed within the rectangular parts in one or two layers with Novozym® 435 yielding two different channel depths (Table 2). The evaluation of the μPBRs was performed under the flow rates ranging from 131.5 μL min^{-1} to 3,756.3 μL min^{-1} to achieve the mean residence times from 0.1 min to 1.4 min. As evident from Figure 5c, very efficient biotransformation process was achieved also μPBR with random packing of particles in two layers, which is a consequence of almost uniform size distribution of the spherical particles allowing for favorable fluid hydrodynamics within the packed bed. Besides, all tested μPBRs performed under laminar flow conditions since Re_p calculated at maximal flow rates for each μPBR using physical properties of *n*-heptane were small, i.e. between 2.47 and 8.37.

To determine the optimum process and operating conditions, the temperature effects on the enzyme-catalyzed transesterification in μPBRs have been examined. It has been reported that the immobilized CaLB in the form of Novozym® 435 is stable at temperatures up to 80 ºC [29,34]. A temperature effect on transesterification reaction was evaluated in a thermostated μPBR with 23.9 mm long, 3.1 mm wide and 0.40 mm deep rectangular channel randomly packed in one layer with 7.1 mg of Novozym® 435 with specific enzyme activity of 133.05 U mg_{CaLB}^{-1},

yielding bed porosity of 0.57 and final enzyme load of 5.53 U μL^{-1} (Table 1). An equimolar 600 mM solution of both substrates in *n*-heptane was continuously pumped through the µPBR yielding τ of 0.1 min. The solvent used in transesterification (*n*-heptane), one substrate (BUT) and the product (BB) have the boiling points at 98.4, 117.6 and 166.7 ºC, respectively [35], so in order to avoid possible problems with sample evaporation, the temperature range tested was from 24 to 80 ºC.

It has been shown that 75 ºC is the optimal temperature. The highest conversion of approximately 81% was achieved at the mean residence time of 0.1 min (data not shown), which is almost 2-fold higher than at 24 ºC. This equals to *BPN* of 11.39 $mmol_{BB}\ g_{CaLB}^{-1}$ and production rate of 4.85 $mmol_{BB}\ h^{-1}$. By comparison, the optimal temperature is close to that of 70 ºC reported by Wang et al. [34].

4.3. Pressure drop in µPBRs of various dimensions

The pressure drop measurements revealed moderate and linearly dependent pressure drops (averaged R^2 = 0.99315 ± 0.004) in the µPBRs along the applied range of flow rates. The highest pressure drop of approximately 88 kPa was measured at the flow rate of 1.8 mL min^{-1} in the µPBR with triangular pre-chambers with the smallest width and depth of 15.8 mm and 0.4 mm, respectively (Figure 3). By comparison, the maximal pressure drop of approximately 42 kPa was measured with the same pressure sensor in the miniaturized packed-bed reactors utilizing LentiKats® at the water flow rate of 1.0 mL min^{-1} [30].

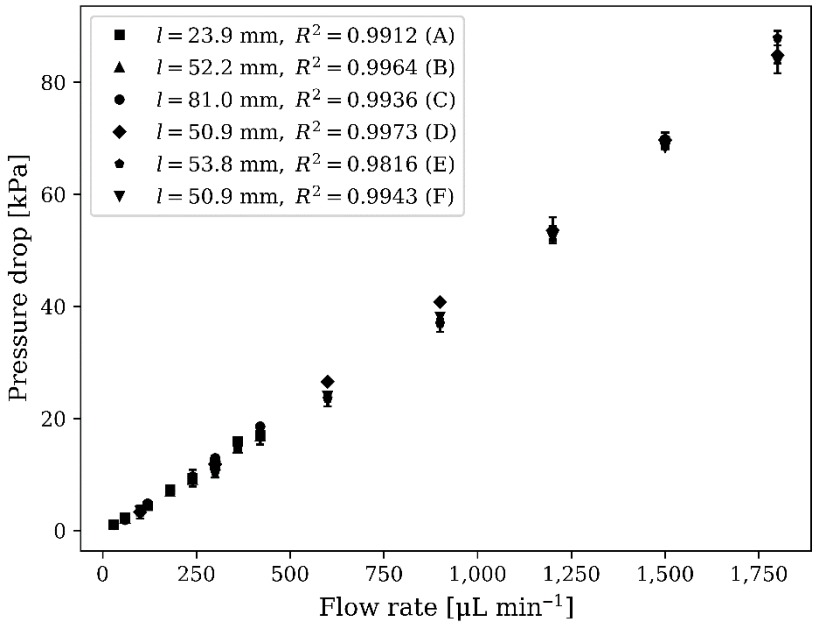

Figure 6. The effect of the flow rate on the pressure drop in the µPBRs without (■, ▲, ●) and with triangular pre-chambers (♦, ▯, ▼) with lengths from 23.9 mm to 81.0 mm as denoted in the legend, widths from 2.9 mm to 29.2 mm and depths from 0.4 mm to 0.8 mm randomly packed with Novozym® 435 (Q = 30–1,800 µL min^{-1}; T = 24 ºC).

The ratio of pressure drops caused by flowing two fluids of different viscosities and densities ($\Delta p_{water}/\Delta p_{heptane} \sim 2.2$) calculated with the Ergun equation [36] was used for the estimation of the pressure drops when using *n*-heptane under the reaction conditions. Stemming from that, a theoretical maximal pressure drop at *n*-heptane flow rate of 1.8 mL min^{-1} would be approximately 40 kPa. For instance, a pressure drop measured by flowing ethanol at the flow rate of 1.0 mL min^{-1} through a microreactor packed with the glass spheres (diameter 53-74 µm) was 560 kPa [36].

5. Conclusions

The LB simulations show that uniform random packing does not affect the RTD results if the bed porosity is kept constant. Despite the small error in mass balance (~1%) LB proved to be a useful tool for RTD analysis. Numerical experiments returned similar results to their physical counterparts. This validation suggests that further use of LB can be made in the future by applying it to the reactor design in the scale-up process. However, an improved collision model and/or improved boundary conditions for solid walls might be considered.

Glucose oxidase biosensor proved as an invaluable tool for RTD experiments as it provides online data of high density. Similar experiments with standard analytical equipment would not be possible as the necessary time and labor consuming sampling would provide insufficient amount of data for RTD analysis.

Pressure drops up to 88 kPa were measured in the μPBRs with different channel shapes and dimensions. Furthermore, μPBRs utilizing Novozym® 435 were evaluated using CaLB-catalyzed synthesis of butyl butyrate as the model reaction. The results of systematic scale-up study shown favorable hydrodynamic conditions and therefore enzyme availability. Further investigations revealed an optimal temperature of 75 °C for CaLB-catalyzed synthesis of butyl butyrate.

Acknowledgements

The financial support of the EC FP7 Project EUROMBR (Grant Agreement No. 608104) and of the Ministry of Education, Science and Sport of the Republic of Slovenia through Grant P2-0191 and PhD Grant MR-39080 (FS) is acknowledged. MB was supported by the Public Scholarship, Development, Disability and Maintenance Fund of the Republic of Slovenia (Grant No. 11011-

73/2013). The support of the COST Action CM1303 Systems Biocatalysis is very much appreciated. Enzyme CaLB in the form of Novozym® 435 was kindly provided by Novozymes A/S (Bagsværd, Denmark). The authors are thankful to coworkers of the University of Ljubljana D. Vrtačnik, B. Pečar, A. Belovič and A. Pajntar for their generous help in the experimental work and T. Urbič for his education on LB modelling.

6. References

[1] K.F. Jensen, Flow chemistry-Microreaction technology comes of age, AIChE J. 63 (2017) 858–869. doi:10.1002/aic.15642.

[2] R. Wohlgemuth, I. Plazl, P. Žnidaršič-Plazl, K. V. Gernaey, J.M. Woodley, Microscale technology and biocatalytic processes: opportunities and challenges for synthesis, Trends Biotechnol. (2015) 1–13. doi:10.1016/j.tibtech.2015.02.010.

[3] P. Žnidaršič-Plazl, Biotransformations in microflow systems: Bridging the gap between academia and industry, J. Flow Chem. (2018) 1–7.

[4] G. Stojkovič, P. Žnidaršič-Plazl, Continuous synthesis of l-malic acid using whole-cell microreactor, Process Biochem. 47 (2012) 1102–1107. doi:10.1016/j.procbio.2012.03.023.

[5] L.H. Andrade, W. Kroutil, T.F. Jamison, Continuous Flow Synthesis of Chiral Amines in Organic Solvents: Immobilization of E. coli Cells Containing Both ω-Transaminase and PLP, Org. Lett. 16 (2014) 6092–6095. doi:10.1021/ol502712v.

[6] N. Pandurić, A. Šalić, B. Zelić, Fully integrated biotransformation of fumaric acid by

permeabilized baker's yeast cells with in situ separation of L-malic acid using ultrafiltration, acidification and electrodialysis, Biochem. Eng. J. 125 (2017) 221–229. doi:doi.org/10.1016/j.bej.2017.06.005.

[7] A. Pohar, P. Žnidaršič-Plazl, I. Plazl, Integrated system of a microbioreactor and a miniaturized continuous separator for enzyme catalyzed reactions, Chem. Eng. J. 189–190 (2012) 376–382. doi:10.1016/j.cej.2012.02.035.

[8] F. Ender, D. Weiser, B. Nagy, C.L. Bencze, C. Paizs, P. Pálovics, L. Poppe, Microfluidic multiple cell chip reactor filled with enzyme-coated magnetic nanoparticles—An efficient and flexible novel tool for enzyme catalyzed biotransformations, J. Flow Chem. 6 (2016) 43–52.

[9] K. Meller, M. Szumski, B. Buszewski, Microfluidic reactors with immobilized enzymes—Characterization, dividing, perspectives, Sensors Actuators B Chem. 244 (2017) 84–106. doi:10.1016/j.snb.2016.12.021.

[10] P.Ž.-P. Marijan Bajić, Igor Plazl, Radek Stloukal, Development of a miniaturized packed bed reactor with ω-transaminase immobilized in LentiKats®, Process Biochem. 52 (2017) 63–72.

[11] A. Faridkhou, J.-N. Tourvieille, F. Larachi, Reactions, hydrodynamics and mass transfer in micro-packed beds—Overview and new mass transfer data, Chem. Eng. Process. Process Intensif. 110 (2016) 80–96. doi:10.1016/j.cep.2016.09.016.

[12] R.W. Pawel Knapkiewicz, Microsensors for Microreaction and Lab-on-a-chip Applications, in: O.V.M. Igor V. Minin (Ed.), Microsensors, InTech, Rijeka, Croatia, 2011: pp. 109–142.

[13] I.B. Tahirbegi, J. Ehgartner, P. Sulzer, S. Zieger, A. Kasjanow, M. Paradiso, M. Strobl, D. Bouwes, T. Mayr, Fast pesticide detection inside microfluidic device with integrated optical pH, oxygen sensors and algal fluorescence, Biosens. Bioelectron. 88 (2017) 188–195. doi:10.1016/j.bios.2016.08.014.

[14] P. Panjan, V. Virtanen, A.M. Sesay, Determination of stability characteristics for electrochemical biosensors via thermally accelerated ageing, Talanta. 170 (2017) 331–336. doi:10.1016/j.talanta.2017.04.011.

[15] A.P.F. Turner, I. Karube, G.S. Wilson, Biosensors : fundamentals and applications, Oxford University Press, 1987.

[16] S. Succi, The Lattice Boltzmann Equation: For Fluid Dynamics and Beyond, Clarendon Press, 2001. doi:ISBN 0198503989.

[17] J.D.T. Sukop, M.C.; Thorne, Lattice Boltzmann Modeling: An Introduction for Geoscientists An Introduction for Geoscientists and Engineers, Springer-Verlag, Berlin, 2006.

[18] C. Guo, Z.; Shu, Lattice Boltzmann Method and Its Applications in Engineering (Advances in Computational Fluid Dynamics), 1st ed., World Scientific Publishing Company, Singapore, 2013.

[19] B. Manz, L.F. Gladden, P.B. Warren, Flow and dispersion in porous media: Lattice-Boltzmann and NMR studies, AIChE J. 45 (1999) 1845–1854. doi:10.1002/aic.690450902.

[20] N. Miložič, M. Lubej, M. Lakner, P. Žnidaršič-Plazl, I. Plazl, Theoretical and experimental study of enzyme kinetics in a microreactor system with surface-immobilized

biocatalyst, Chem. Eng. J. 313 (2017) 374–381.

[21] P. Žnidaršič-Plazl, I. Plazl, Modelling and experimental studies on lipase-catalyzed isoamyl acetate synthesis in a microreactor, Process Biochem. 44 (2009) 1115–1121. doi:10.1016/j.procbio.2009.06.003.

[22] T. Zeiser, P. Lammers, E. Klemm, Y.W. Li, J. Bernsdorf, G. Brenner, CFD-calculartion of flow, dispersion and reaction in a catalyst filled tube by the lattice Boltzmann method, Chem. Eng. Sci. 56 (2001) 1697–1704. doi:10.1016/S0009-2509(00)00398-5.

[23] H.H. Freund, T. Zeiser, F. Huber, E. Klemm, G. Brenner, F. Durst, G. Emig, Numerical simulations of single phase reacting flows in randomly packed fixed-bed reactors and experimental validation, Chem. Eng. Sci. 58 (2003) 903–910. doi:10.1016/S0009-2509(02)00622-X.

[24] S.P. Sullivan, F.M. Sani, M.L. Johns, L.F. Gladden, Simulation of packed bed reactors using lattice Boltzmann methods, Chem. Eng. Sci. 60 (2005) 3405–3418. doi:10.1016/j.ces.2005.01.038.

[25] O. Levenspiel, Tracer technology, Springer Science+Business Media, 2012. doi:10.1007/978-1-4419-8074-8.

[26] N. Márquez, P. Castaño, M. Makkee, J.A. Moulijn, M.T. Kreutzer, Dispersion and holdup in multiphase packed bed microreactors, Chem. Eng. Technol. 31 (2008) 1130–1139. doi:10.1002/ceat.200800198.

[27] M. Coblyn, A. Truszkowska, G. Jovanovic, Characterization of microchannel hemodialyzers using residence time distribution analysis, J. Flow Chem. 6 (2016) 53–61. doi:10.1556/1846.2015.00041.

[28] O. Levenspiel, Chemical Reaction Engineering, 3rd ed., John Wiley & Sons, Inc., New York, 1999.

[29] I. Denčić, S. De Vaan, T. Noël, J. Meuldijk, M. De Croon, V. Hessel, Lipase-based biocatalytic flow process in a packed-bed microreactor, Ind. Eng. Chem. Res. 52 (2013) 10951–10960. doi:10.1021/ie400348f.

[30] P.Ž.-P. M. Bajić, I. Plazl, R. Stloukal, B. Pečar, D. Vrtačnik, Development and characterization of miniaturized packed bed reactors, in: D.R. D. Vrtačnik, M. Topič (Ed.), 52nd Int. Conf. Microelectron. Devices Mater. with Work. Biosens. Microfluid., MIDEM Society for Microelectronics, Electronic Components and Materials 1000 Ljubljana, Stegne 7, SLOVENIA, 2016: pp. 116–121.

[31] Q. Zou, X. He, On Pressure and Velocity Boundary Conditions for the Lattice Boltzmann BGK Model, Phys. Fluids. 9 (1997) 1591. doi:10.1063/1.869307.

[32] M. Hecht, J. Harting, Implementation of On-Site Velocity Boundary Conditions for D3Q19 Lattice Boltzmann Simulations, J. Stat. Mech. Exp. (2010).

[33] T. Krüger, H. Kusumaatmaja, A. Kuzmin, O. Shardt, G. Silva, E.M. Viggen, The Lattice Boltzmann Method: Principles and Practice, Springer International Publishing, 2017. https://books.google.at/books?id=S-d0DQAAQBAJ.

[34] J. Wang, S.S. Gu, H.S. Cui, X.Y. Wu, F.A. Wu, A novel continuous flow biosynthesis of caffeic acid phenethyl ester from alkyl caffeate and phenethanol in a packed bed microreactor, Bioresour. Technol. 158 (2014) 39–47. doi:10.1016/j.biortech.2014.01.145.

[35] NCBI, PubChem Compound Database. Bethesda, National Center for Biotechnology Information (database), (2004).

[36] M.W. Losey, M. a Schmidt, K.F. Jensen, Microfabricated Multiphase Packed-Bed Reactors: Characterization of Mass Transfer and Reactions, (2001) 2555–2562.

Appendix A. Nomenclature

Latin symbols

BPN	biocatalyst productivity number [$mmol_{BB}\, g_{CaLB}^{-1}$]
c	lattice speed of sound [–]
C	tracer concentration [–; mM]
C_{max}	maximal concentration at the outlet [–; mM]
C_{CaLB}	concentration of CaLB [$g_{CaLB}\, L^{-1}$]

C_{glu}	glucose concentration [mM]
C_{N435}	concentration of Novozym® 435 [g_{N435} L^{-1}]
d	channel depth [mm]
D	molecular diffusivity [m^2 s^{-1}]
$\mathfrak{D}$	axial dispersion coefficient [m^2 s^{-1}]
d_{N435}	average diameter of Novozym® 435 [m; µm]
$\boldsymbol{e}$	basic lattice velocity [–]
f	distribution function [–]
f^{eq}	equilibrium distribution function [–]
g	distribution function [–]
g^{eq}	equilibrium distribution function [–]
l	channel length [mm; m]
PR	production rate [$mmol_{BB}$ h^{-1}]
Q	volumetric flow rate [µL min^{-1}]
Q_P	volumetric productivity [$mmol_{BB}$ L^{-1} min^{-1}]
Re_p	particle Reynolds number [–]
s	skewness [–]
Sc	Schmidt number [–]
t	time [min]

t_0	time [min]
t/τ	dimensionless time [–]
T	temperature [ºC]
$\boldsymbol{u}$	local velocity [–]
V	volume of empty reactor [µL]
v	fluid velocity [m s^{-1}]
v_i	mean superficial fluid velocity [m s^{-1}]
V_v	reactor void volume [µL]
w	channel width [mm]
W	lattice weight factor [–]
$\widetilde{W}$	modified lattice weight factor [–]
$\boldsymbol{x}$	space coordinates [–]
X	conversion [%]

Greek symbols

γ_{CaLB}	enzyme load [U μL^{-1}]
$\Delta p_{heptane}$	pressure drop when flowing *n*-heptane [Pa]
Δp_{water}	pressure drop when flowing water [Pa]

ε	bed porosity [–]
η	fluid dynamic viscosity [Pa s]
ρ	local density [–]
ρ_f	fluid density [kg m^{-3}]
ρ_s	local solute concentration [–]
ν	kinematic viscosity [–]
σ^2	variance [s^2; min^2]
τ	mean residence time [min]
ω	solvent's relaxation parameter [–]
ω_s	solute's relaxation parameter [–]

Abbreviations and acronyms

ACE	acetaldehyde
BB	butyl butyrate
BKG	Bhatnagar–Gross–Krook
BSA	bovine serum albumin
BUT	1-butanol
CaLB	*Candida antarctica* lipase B

CFD	computational fluid dynamics
D3Q19	3D LB model with 19 lattice velocities
D3Q7	3D LB model with 7 lattice velocities
GOx	glucose oxidase from *Aspergillus niger* VII S
GPU	graphics processing unit
ID	inner diameter
LB	lattice Boltzmann
µPBR	micro packed-bed reactor
N435	Novozym® 435
OD	outer diameter
PBS	phosphate buffered saline
PEEK	polyetheretherketone
PFA	perfluoroalkoxy
PMMA	poly(methyl methacrylate)
PTFE	polytetrafluoroethylene
RTD	residence time distribution
VB	vinyl butyrate

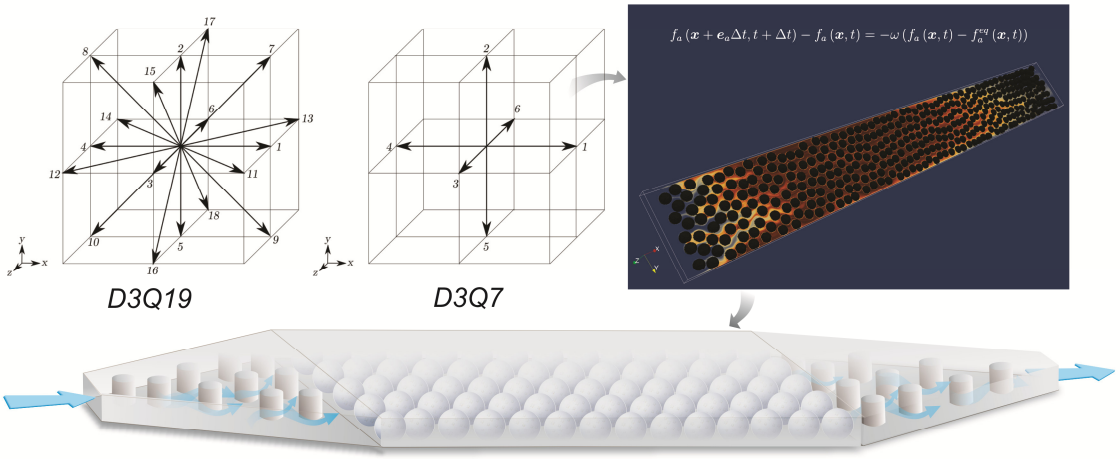

Highlights

- A micro packed-bed reactor was theoretically and experimentally characterised.
- A residence time distribution (RTD) was predicted by lattice Boltzmann method.
- Numerical simulations were in good agreement with biosensor-based RTD experiments.
- A reactor with immobilized lipase B was very efficient for selected esterification.
- Very efficient scale-up of the packed-bed reactor enabled high productivities.